TM-1065
1620

Fermilab

PRELIMINARY STUDY OF HIGH FIELD DIPOLE MAGNET

Kenji Ishibashi and A.D.McInturff

August 25, 1981

ABSTRACT

A study was made on design of a shell-type dipole magnet with an operational field of 10T. Optimization was made for superconducting cable and magnet dimensions. Magnetic (Lorentz) forces were computed and compared with other dipole magnets. Displacement and stress analysis with the help of a simplified model calculation was numerically made for windings and collars. Feasibility of high field magnet of inner diameter of two inches was examined.

- - - - - - - -

Many superconducting dipole magnets have recently been constructed successfully for central fields ranging from 4 to 5T at various laboratories around the world. The fabrication techniques and parameters such as preload and conductor insulation are almost established for magnets in this field range. The next logical step for development of dipole magnets would be to have a higher central field, for example, 10T. The higher field would lead to a higher particle beam energy in a given area of an accelerator site. These high field magnets may be obtained in the near future by relatively high current density supconductor[1] realizable in the solid solution alloys such as NbTi and NbTiTa at the field level of 10T at superfluid helium temperature. Since there is, of course, a limitation of critical current density even at these temperatures, the windings of 10T magnets will, in general, be larger than magnets in the range of 4 to 5T for a given beam aperture. It is, therefore, very important from an economic point of view to decrease the beam aperture and increase the superconductor's critical current density. For an accelerator in the "Pentavac" project, the particle beam energy will be injected near 1 TeV, and accordingly the beam size will be reduced to 3/4 of that of the injected Energy Saver (E/S) beam project, although the exact beam size in the Pentavac depends

on the accelerator design and the E/S final beam. Taking advantage of this possible small beam size, parameterization study was made for four shell-type magnets varying as parameters, the number of strands per shell, magnet inner diameter, and supporting collar geometry.

1. MAGNETIC PROPERTIES

1.1 Number of strands in cable.

Examples of critical current density of binary (NbTi) and ternary (NbTiTa) alloys are shown in Figure 1 for a temperature of 1.8K. A dashed line for NbTi shows typical critical current density[1] of superconductor for the Fermilab E/S project. The upper solid line indicates excellent critical current density which can be obtained by careful selection of this conductor. The lower solid line for NbTi stands for a selected poor conductor, and this current density was taken to be 10% lower than that of the dashed line. The dashed line for NbTiTa shows published data on Nb-Ti-25wt%Ta by MCA. The solid line for NbTiTa indicates critical current density which is thought to be realized by further study on the basis of present measured values for NbTi.* Although there is a program to increase critical current density by further optimization of metallurgical variables at high field of binary and ternary alloys, their anticipated results are not considered in this study. The increased critical current density would effect the study in two areas, first is to reduce the number of strands per cable and second, (possibly) increase the volume fraction of copper to superconductor (max 1.6→1.8/1).

The highest field at each shell at the central field of 10T is shown in Figure 1, with four types of marks for a typical high field magnet of 2.25 inch i.d. The star, square, triangular and circular marks stand for the highest field at the inside (first), second, third and fourth shells, respectively. Taking into considera-

*Actually recent data from Japan[2] has shown NbTi at 11T, 1.8K, is able to achieve a critical current density of 130kA/cm^2.

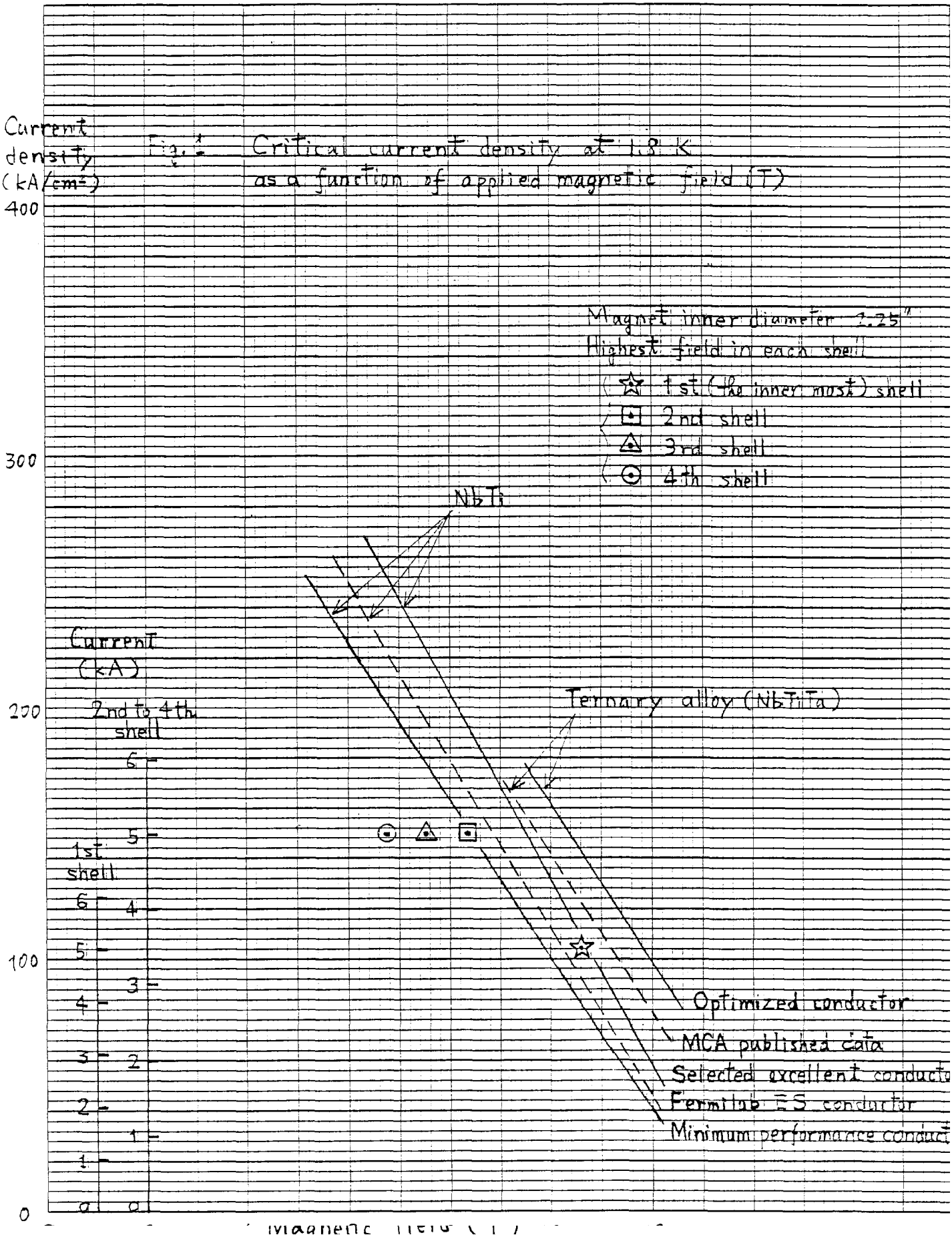
Current density (kA/cm²)
Fig. 1 Critical current density at 1.8 K as a function of applied magnetic field (T)
400
300
200
100
0
Magnet inner diameter 1.25"
Highest field in each shell
1st (the inner most) shell
2nd shell
3rd shell
4th shell
NbTi
Ternary alloy (NbTiTa)
Current (kA)
2nd to 4th shell
1st shell
6
5
4
3
2
1
0
Optimized conductor
MCA published data
Selected excellent conduct
Fermilab ES conductor
Minimum performance conduct
Magnetic field (T)

tion the high field point distribution, the ternary alloy is needed only for the inner shell, and the number of strands in the cable were determined to be 33 for the inner shell and 23 for the other ones. Conductor specifications are listed in Table I. The additional ordinates in Figure 1 show the transport current which corresponds to the superconductor current density in cables of 33 and 23 strands. The NbTiTa conductor shown by the solid line is used for the inside shell, and the excellent and poor NbTi conductors are used for the second and fourth shells, respectively. The designed operational currents correspond to about 80% of critical current density at the highest field at each shell. Since the critical current of cable is usually about 10% lower than the sum of critical currents of its component strands, the operational current of cable corresponds to about 90% of the critical current of the cable.

As shown in Table I, no epoxy glass tape is used as an insulator.[3] The insulation, consisting of Kapton and Mylar film, has two advantages. The first advantage, geometry, is to increase the overall current density of the winding, and the second is to increase elastic modulus of the winding to 6Mpsi at cryogenic temperature.

1.2 Magnet characteristics.

Parameters for magnet windings which were used for the above determination of number of strands are listed in Table II for three sizes of magnets (diff. i.d., 2.0, 2.25 and 2.5 inch). Because these three windings have similar angular turn distributions, there is very little difference in the highest field seen at each shell between the three winding sizes.

Characteristics for the three different size high field magnet windings are shown in Figure 2 and given in Table II as a function of iron inner radius. The letters A, B and C correspond to the magnet inner radii of 2.0, 2.25 and 2.5 inches, respectively. Arrows at

TABLE I

CONDUCTOR

	Inner Shell	Other Shells
Strand		
Superconductor	NbTiTa	NbTi
Critical current density	130kA/cm^2 at 11T, 1.8K	~180kA/cm^{2}at 8T, 1
Filament diameter	8μm	8μm
Copper/Superconductor	1.5	1.5
Strand diameter	0.0268 in.	0.0267 in.
Twist pitch	0.5 in.	0.5 in.
Cable		
Number of strands	33	23
Critical current	5.5kA at 11T, 1.8K	~5.4kA at 8T, 1.8
Nominal width	0.440 in.	0.307 in.
Nominal thickness	0.0495 in.	0.0495 in.
Insulation		
Kapton film	0.001 in. thick, spiral wrap with 20% gap	
Mylar film	0.002 in. thick, spiral wrap covering the gap of Kapton	
Elastic Modulus	3Mpsi at room temp. 6Mpsi at liq. nitrogen temp.	3Mpsi at room tem 6Mpsi at liq. nitrogen temp.

TABLE II

MAGNET WINDING

	Magnet inner diameter (in.) 2.0	2.25	2.5
Winding			
n_1	30	34	37
n_2	28	31	34
n_3	25	26	27
n_4	27	28	29
r_i (in.)	1.0	1.125	1.25
r_2	1.459	1.594	1.716
r_3	1.791	1.923	2.044
r_4	2.122	2.253	2.372
θ_1 (deg.)	76.59	76.75	76.96
θ_2	53.24	54.72	56.45
θ_3	39.45	38.63	38.17
θ_4	36.40	35.90	35.66
t (in.)	0.005	0.005	0.005
Iron			
R	4.6	4.9	5.25
W	20	22	24
H	15	16	18

n_i = Number of layers

r_i = Inner radius of shell

θ_i = Maximum angle

t = Insulator thickness on the median plane

R = Inner diameter of iron

W = Width of iron

H = Height of iron

i = Shell number

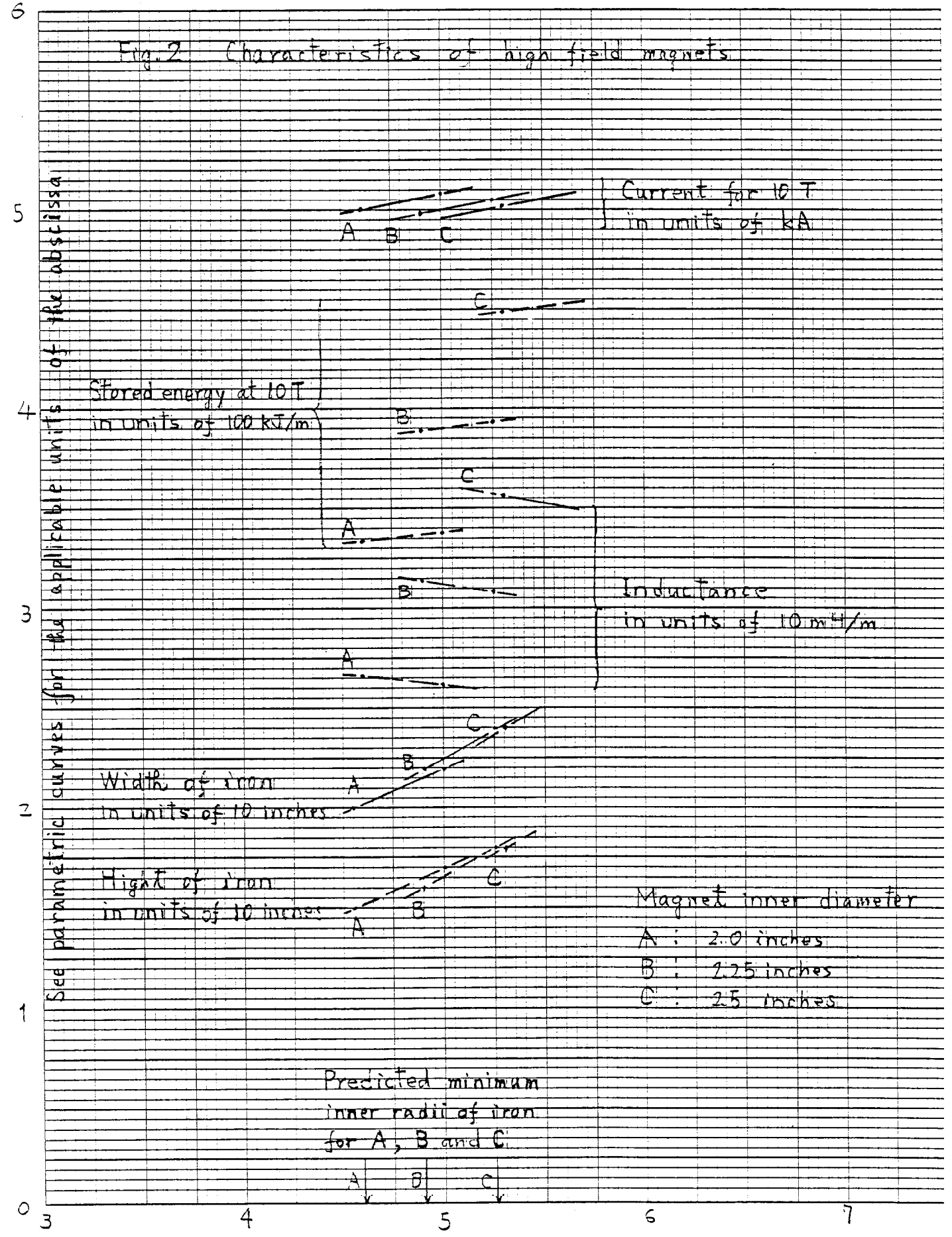
Fig. 2 Characteristics of high field magnets
See parametric curves for the applicable units of the abscissa
Current for 10 T in units of kA
A B C
Stored energy at 10 T in units of 100 kJ/m
Inductance in units of 10 mH/m
Width of iron in units of 10 inches
Hight of iron in units of 10 inches
Magnet inner diameter
A : 2.0 inches
B : 2.25 inches
C : 2.5 inches
Predicted minimum inner radii of iron for A, B and C
0
1
2
3
4
5
6
3
4
5
6
7

the abscissa indicate the iron inner radii which correspond to the iron parameters in Table II and were obtained by adding an inch to the outer radii of collars described later. This represents the cryostat space.

Transport currents for the central field of 10T are 5.0 to 5.05kA and slightly dependent on the inner radius of the iron. Stored energy/unit length at 10T depend primarily on magnet size (i.d.), and it can be as low as 330kJ/m for a 2 inch i.d. magnet. Inductance is similarly dependent on the inner diameter of the magnet. The dimensions of the iron are given in Figure 2 as well. The width and height of iron for the 2.0 inch i.d. magnet, for example, are 20 and 16 inches, respectively.

1.3 Harmonic content.

Harmonic coefficients in the straight section obtained for the configuration in Table II, with assumption of infinite permeability of iron, are shown in Figure 3. Circular, square and triangular marks stand for magnet inner diameters of 2.0, 2.25 and 2.5 inches, and the solid and dashed marks stand for radius of normalization of 1 inch and 2 cm, respectively, of harmonic coefficients. The accelerator for Pentavac will have very high energy-injected particle beams, and the normalization radius which is applicable for determining field homogeneity affecting the particle is thought to be below 2 cm. The solid and dashed square marks (magnet i.d. = 2.25 inches) are connected by solid and dashed lines, respectively, for ease of interpretation. The 2 cm normalization radius for the high field magnets is thought to be as stringent as that of 1 inch for the E/S magnets and have the same physical significance.

The sextupole harmonic coefficient was chosen to have a large positive value in order to cancel that of the end windings. The decapole coefficient was de-

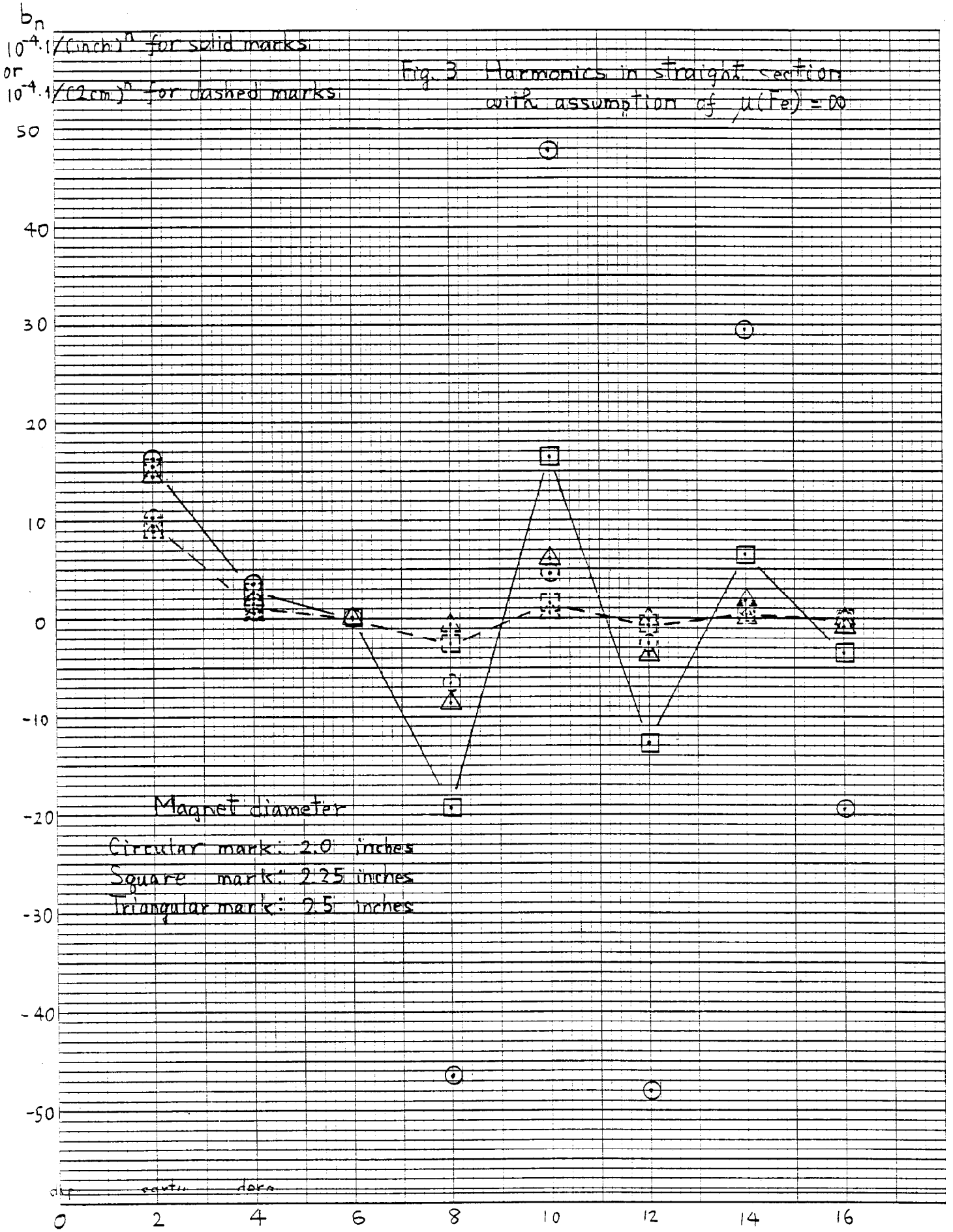

Fig. 3 Harmonics in straight section with assumption of $\mu(Fe) = \infty$

Magnet diameter
Circular mark: 2.0 inches
Square mark: 2.25 inches
Triangular mark: 2.5 inches

signed to have a positive value for the same reason. The co-efficient of 14-pole was simply adjusted as close to zero as possible.

The effect of changes of azimuthal arc length of winding on harmonic coefficients is presented in the Appendix. In Figure 4 all arc lengths of all shells are assumed to be decreased by the same value of 4 mils. If the normalization radius is taken as 2 cm, or approximately the same percentage of aperture, the change in harmonic coefficients is comparable to those of the E/S dipole magnets. Figure 5 shows standard variations of harmonic coefficients due to the random changes of all arc lengths of 4 mils.

Effects of horizontal displacement of the windings are shown in Figure 6 and 7. All shells are assumed to move outward by the same amount in Figure 6. All shells are assumed to exist outward or inward around the design positions with a random variation of 4 mils in Figure 7. When normalized for similar percent of aperture; i.e., 2 cm, the sensitivity of harmonic coefficients is similar to those of the present E/S dipole magnets.

A cross sectional view of the winding is shown in Figure 8 for the 2.25 inch i.d. magnet. Other designs[4,5] for high field magnets and also presently existing magnets[6] are shown for comparison of the resulting dimensions. Figure 9 shows cross sectional views of the corresponding iron yokes of each design.

2. MECHANICAL CONSIDERATIONS

2.1 Magnetic force.

The magnetic pressure experienced by the presently designed high field magnet at 10T is shown in Figure 10. The compressive pressure on the median plane of the inside shell is 12.7 kpsi and approximately twice as high as that of the present E/S dipole magnets. While the magnetic field in the inner shell of the high field magnet is higher than that of the second shell, the overall current density of the inner shell is 33kA/cm^2 and lower than that of the second shell, 45kA/cm^2. This results

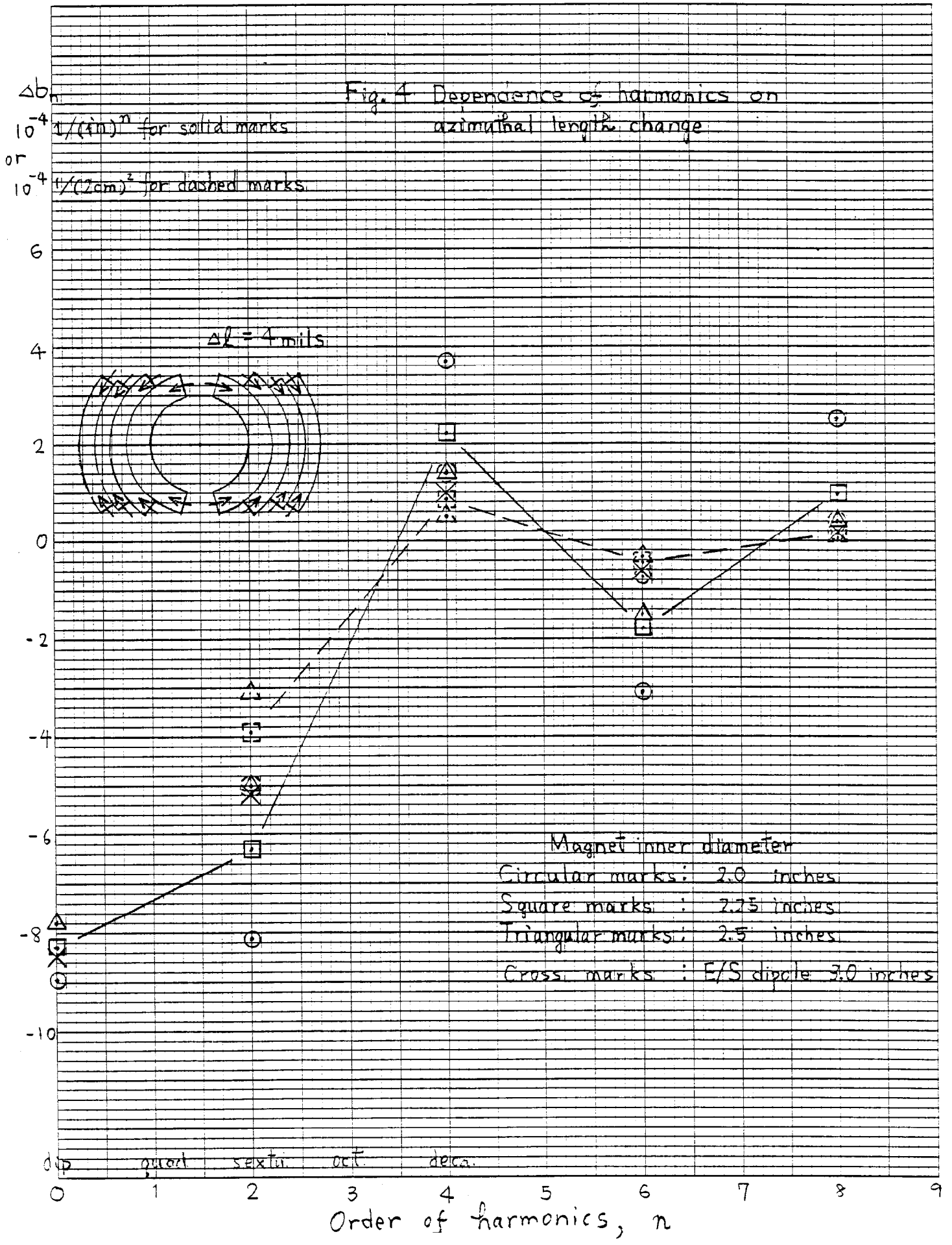
Fig. 4 Dependence of harmonics on azimuthal length change
Δb_n
10^{-4} $1/(4m)^n$ for solid marks
or
10^{-4} $1/(2cm)^2$ for dashed marks
$\Delta\ell$ = 4 mils
6
4
2
0
-2
-4
-6
-8
-10
Magnet inner diameter
Circular marks: 2.0 inches
Square marks: 2.25 inches
Triangular marks: 2.5 inches
Cross marks: E/S dipole 3.0 inches
dip
quad
sextu
oct
deca.
0
1
2
3
4
5
6
7
8
9
Order of harmonics, n

$\sigma_{tot} = \sqrt{\sigma_{b_n}^2 + \sigma_{a_n}^2}$

$10^{-4} \cdot 1/(\text{inch})^n$ for solid marks

or

$10^{-4} \cdot 1/(2\text{cm})^n$ for dashed marks

Fig. 5 Dependence of harmonics on random azimuthal length change

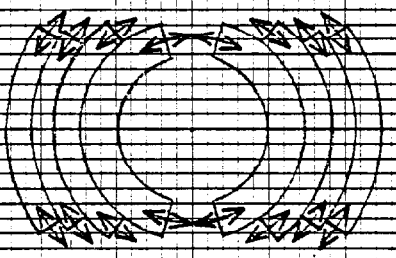

Magnet inner diameter

Circular marks: 3.0 inches

Square marks: 2.25 inches

Triangular marks: 2.5 inches

Cross marks: E/S dipole 3.0 inches

dip. quadru. sextu. oct. deca.

Order of harmonics, n

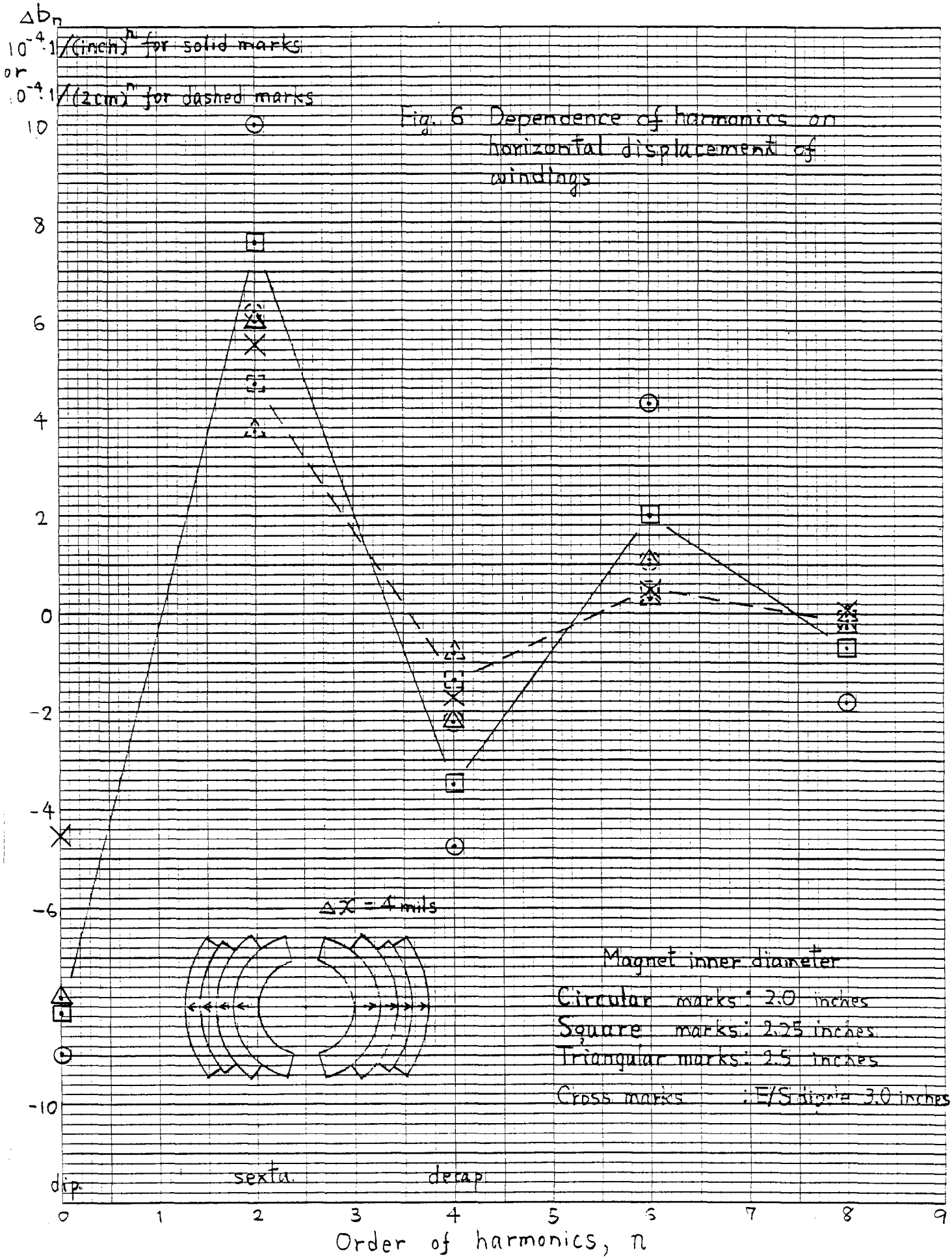

Fig. 6 Dependence of harmonics on horizontal displacement of windings

$\sigma_{tot} = \sqrt{\sigma_{b_n}^2 + \sigma_{a_n}^2}$

$10^{-4} \cdot 1/(\text{inch})^n$ for solid marks

or

$10^{-4} \cdot 1/(2\text{cm.})^n$ for dashed marks

Fig. 7 Depence of harmonics on random horizontal displacement of shells

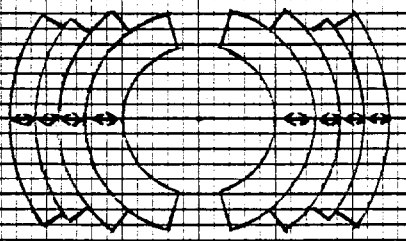

Magnet inner diameter

Circular marks: 2.0 inches

Square marks: 2.25 inches

Triangular marks: 2.5 inches

Cross marks: E/S dipole 3.0 inches

10
9
8
7
6
5
4
3
2
1
0

0 1 2 3 4 5 6 7 8 9

Order of harmonics, n

Fig. 8 Windings and collars of high field magnets and magnet designs.

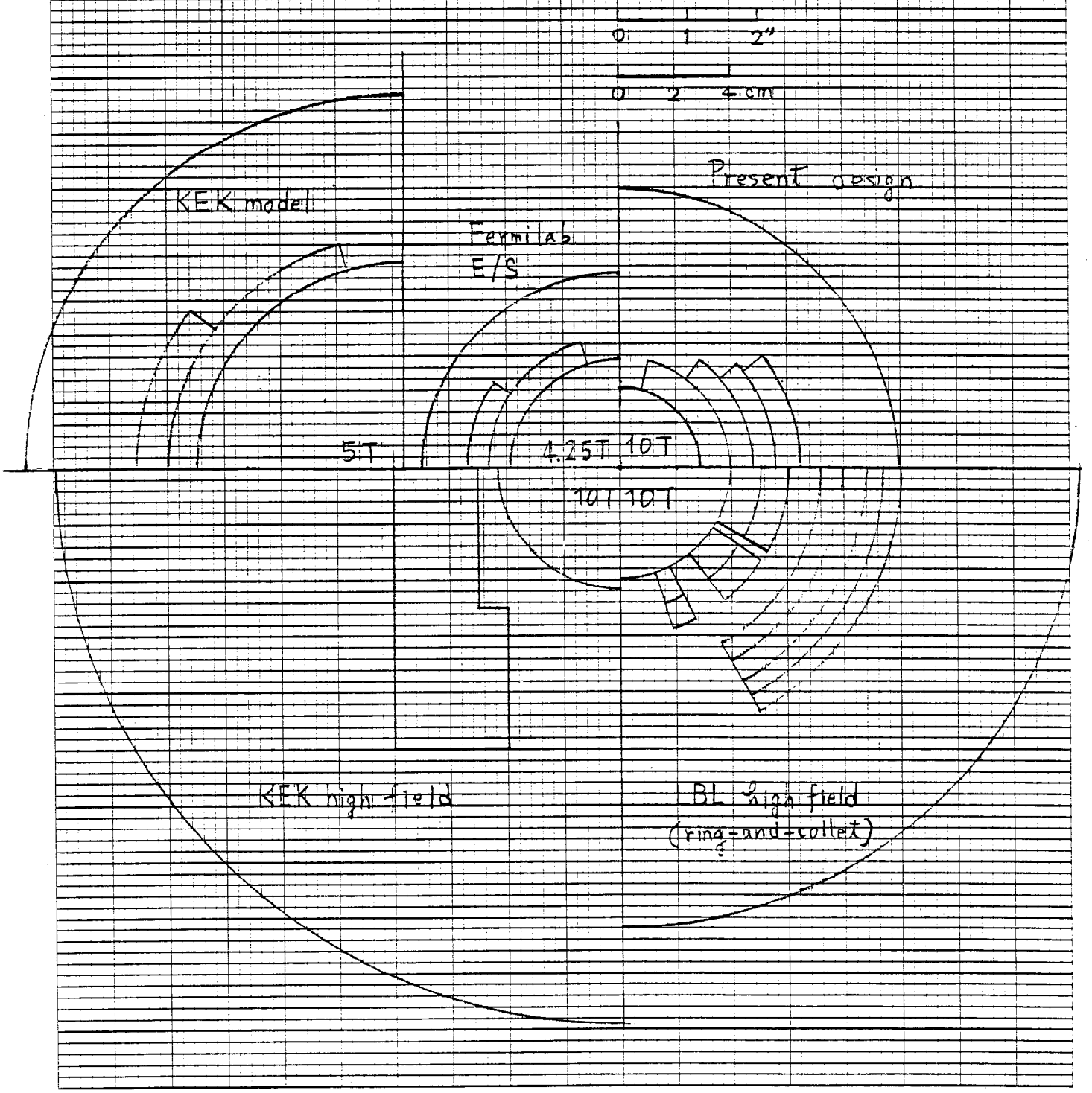

Fig. 7 Iron of high field magnets and magnet designs

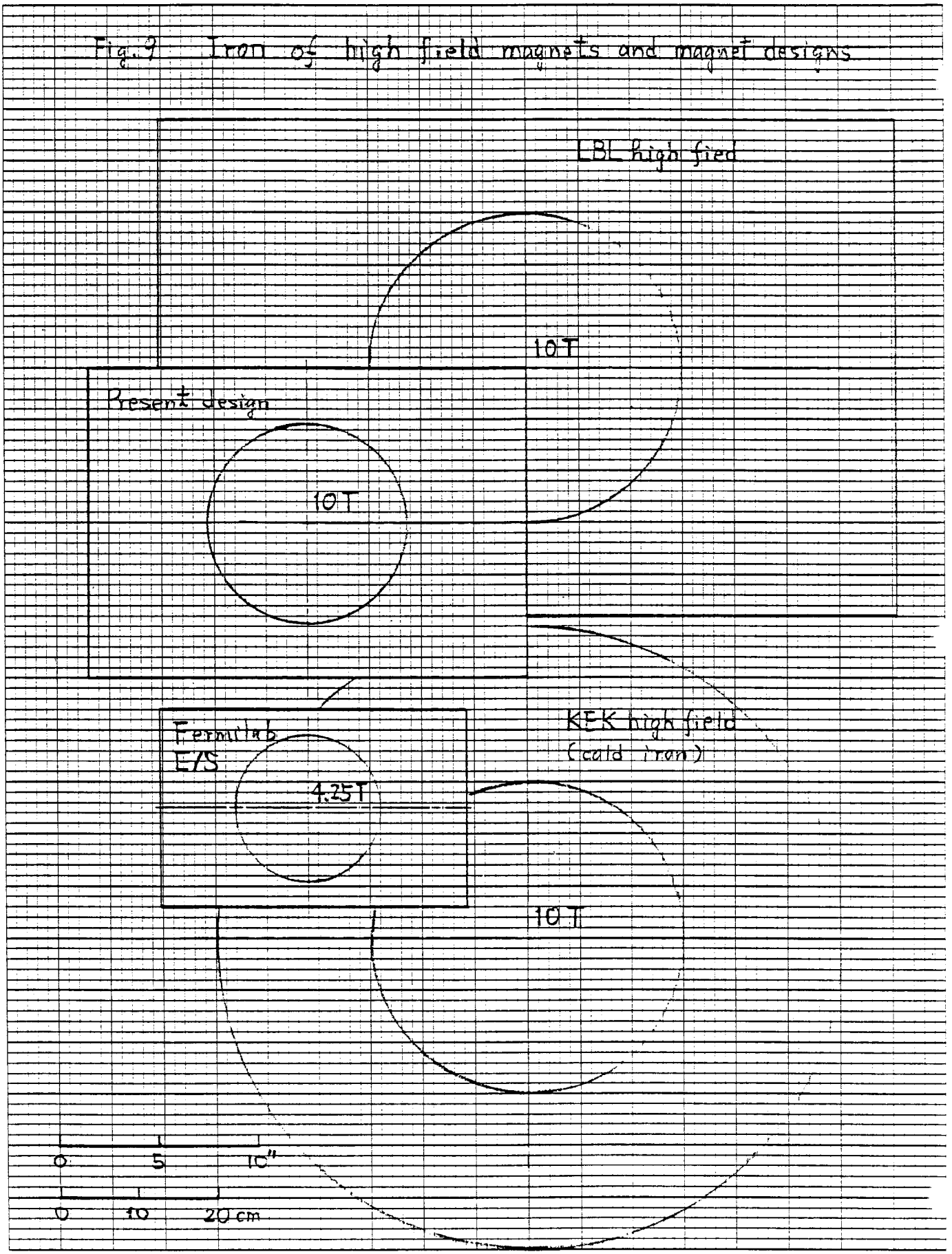

Fig. 10 Electromagnetic pressure of a high field magnet

Current : 5.0 kA
Central field : 10 T
Inner diameter : 2.25"

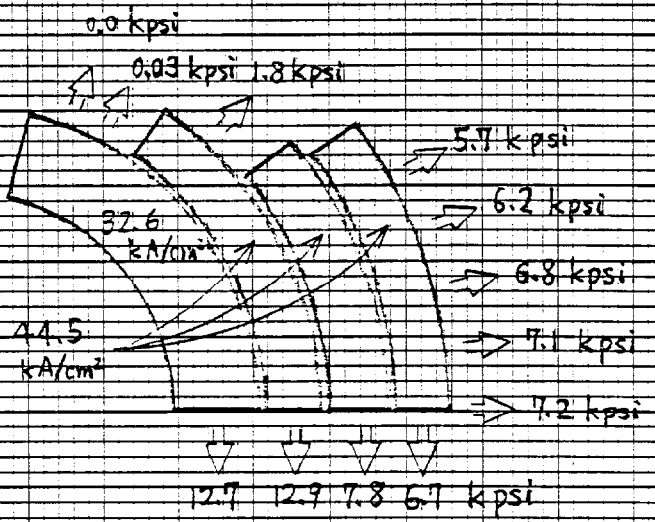

in the second shell having a comparable compressive pressure at the median plane to the inner shell.

Table III lists the compressive pressure[4,5,6] on the median plane due to the magnetic force of various designs. The pressure of the inner shell of the present design is the highest of the three high field dipole magnet designs listed. The compressive pressure of the KEK high field dipole magnet design is lower because of its winding geometry, picture frame. A LBL high field dipole magnet design results in a value of 6.6kpsi by use of an elaborate "compartment" scheme enabling the force not to be transmitted through the whole shell azimuthally.

One KEK model dipole is quite informative, in particular because it has a shell-type winding and its compressive pressure on the median plane of the inner shell is 13.3kpsi at a central field of 5T. This pressure is slightly higher than that of the proposed magnet design at 10T. The high pressure of the KEK model dipole magnet comes from its large inner diameter, 5.51 inches. This KEK model dipole was excited in pressurized helium II at a temperature of 1.8K. The central field was increased by about 30% and reached 6.7T. Because the transport current exceeded the current limit of the power supply, the excitation was stopped at this field. The performance corresponds to a peak compressive pressure of 24.9kpsi. These results lead us to conclude that the compressive pressure of the present proposed design is probably not a critical parameter.

Figure 11 shows the compressive forces on the median plane as a function of magnet inner diameter. Triangular marks stand for total compressive force (sum of forces on the right and left halves of the winding), and circular marks stand for compressive pressure on the median plane of the inner shell. The total compressive force of the present proposed design is slightly higher than that of the KEK model dipole magnet excited at 6.7T.

TABLE III

PRESSURE ON THE MEDIAN PLANE DUE TO MAGNET FORCE

Magnet	Pressure of the inner shell (kpsi)	Max. pressure in all shells (kpsi)	Central field (T)	Inner diam. (in.)	Winding type
Present design	12.7	12.9	10.0	2.25	4 shells
KEK high field dipole	(5.7)*	8.2 (9.4)**	10.0	(3.44)***	picture frame
LBL high field dipole	6.6	16.8	10.0	3.15	6 shells
E/S dipole†	6.0	6.0	4.3	3.0	2 shells
KEK model dipole†	13.3	13.3	5.0	5.51	2 shells
	24.9	24.9	6.7	Temperature 1.8K	

† = Presently fabricated magnets.

* = Compressive pressure on the notch which is a part of the median plane.

** = Maximum bursting pressure is higher than the maximum compressive pressure on the median plane.

*** = Horizontal length between right and left half windings on the median plane.

Fig. 11 Compressive electromagnetic force on the median plane

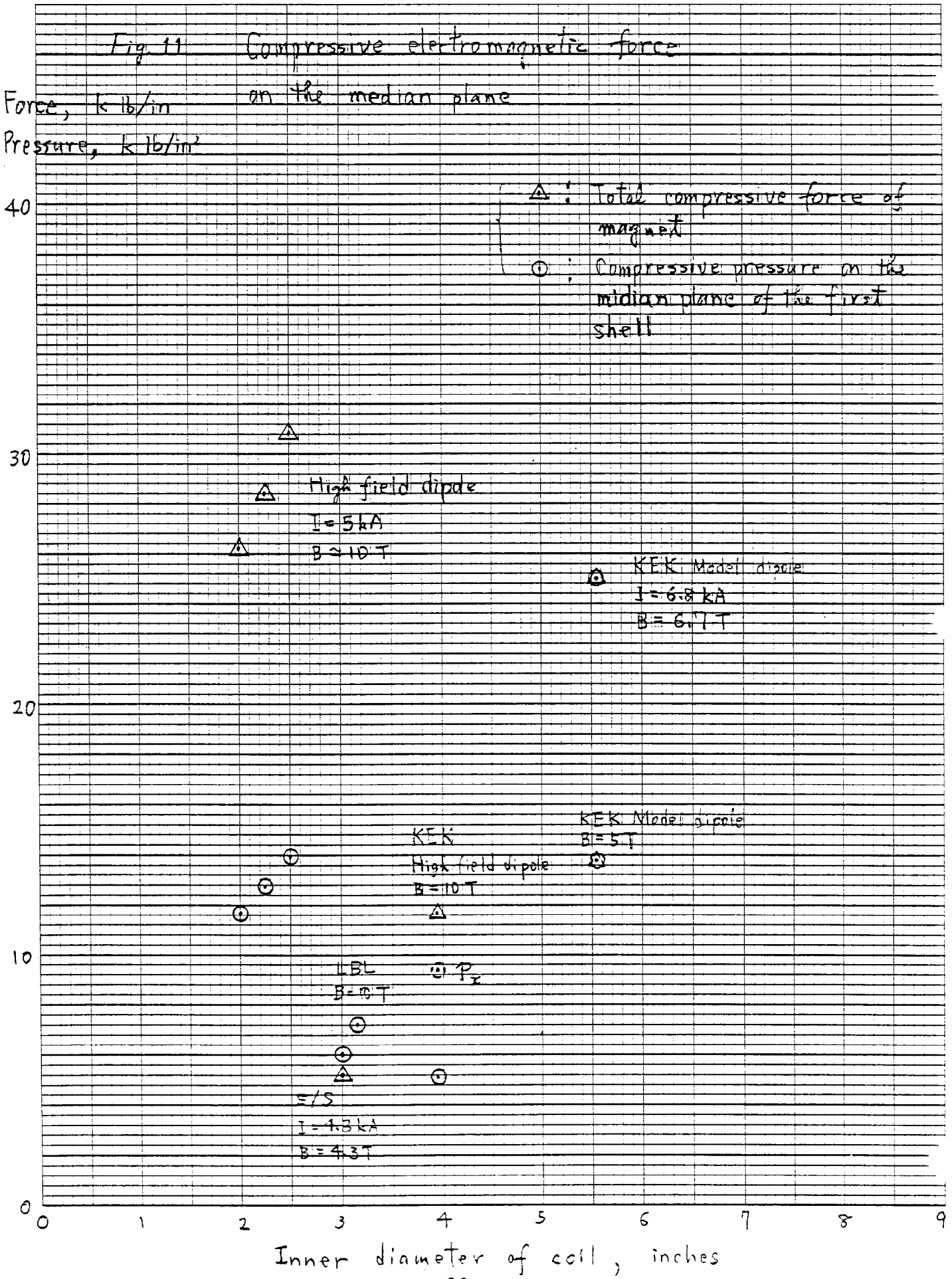

Bursting forces are plotted in Figure 12. The present proposed design gives a similar total bursting force as that sustained by the KEK model dipole at 6.7T. Figures 11 and 12 show that the magnetic field distribution in the picture frame magnet gives a larger bursting force than the vertically compressive one.

2.2 Displacement of the shell-type dipole magnets.

A stress analysis computer code, ANSYS, was used to determine mechanical behavior of windings. Prior to analysis of the proposed high field magnet, a calculation was made for the E/S dipole magnet for comparison with actual data. An example of computational geometry used, is shown in Figure 13, where the E/S dipole magnet is approximated by quadrilateral meshes. These elements, which have the property of taking into account the contact surface for regions between inner and outer shells and between shell and collar, were used.

The actual collar is not a complete ring and the upper and lower halves are connected through punched holes and by welding. Two kinds of calculations (cases A and B) were made for the purpose of checking the validity of the approximation of the geometry. As shown in Figure 14, case A indicates that the collar is made of a complete ring. Case B indicates that the connection between upper and lower halves is not made. The two halves were fixed on the top and bottom points to prevent them from bursting apart.

The results of the calculations are shown by the triangular marks for case A and circles for case B. The actual displacement of E/S dipole magnets is about 3 mils at a current of 4000A. The value in case A is close to this displacement and accordingly the boundary condition corresponding to case A approximates the actual displacement. Results of calculations for the KEK model dipole magnet are also shown for case A. A

Fig. 12 Total bursting electromagnetic force

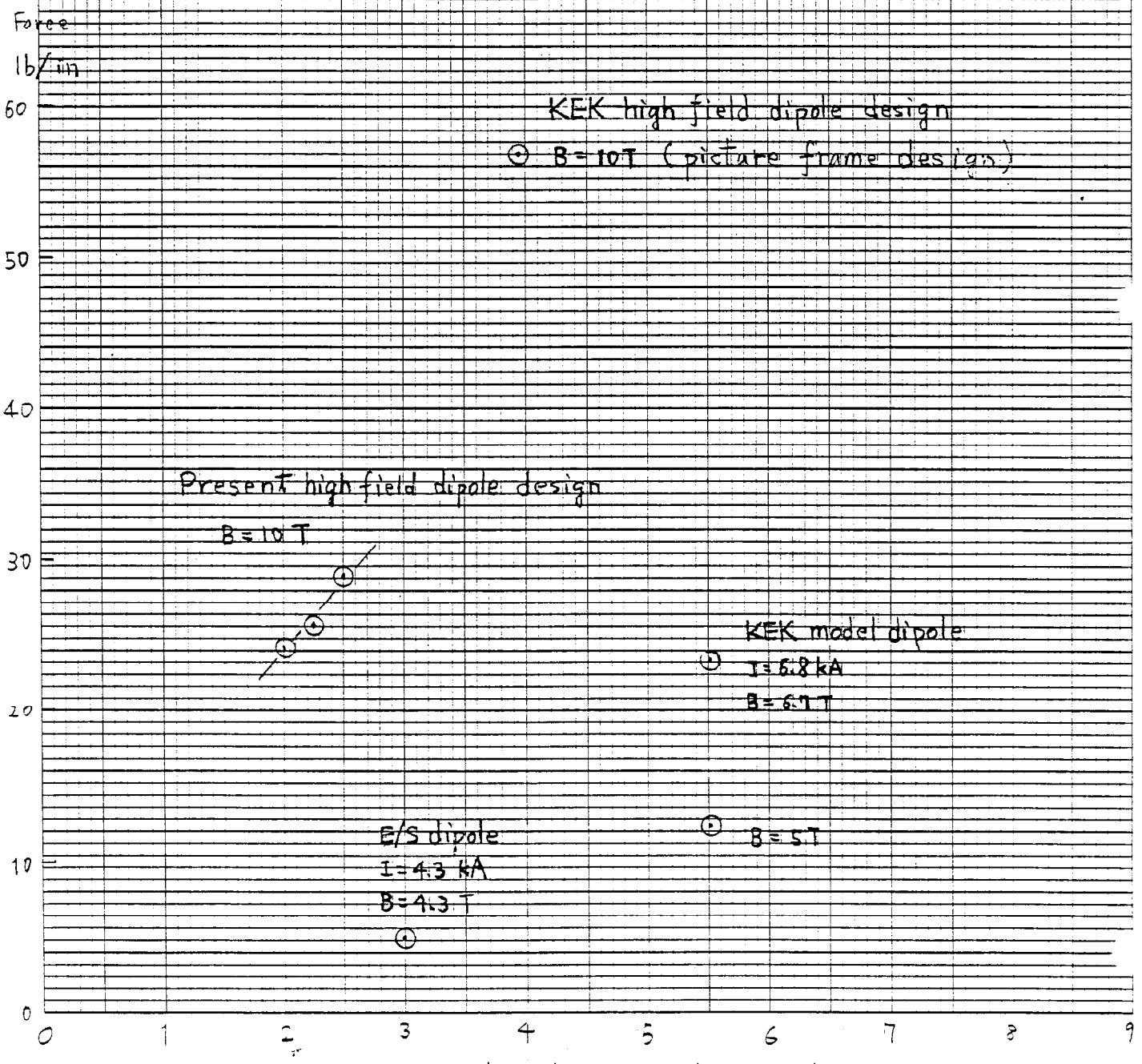

Fig. 13 E/S Dipole Magnet

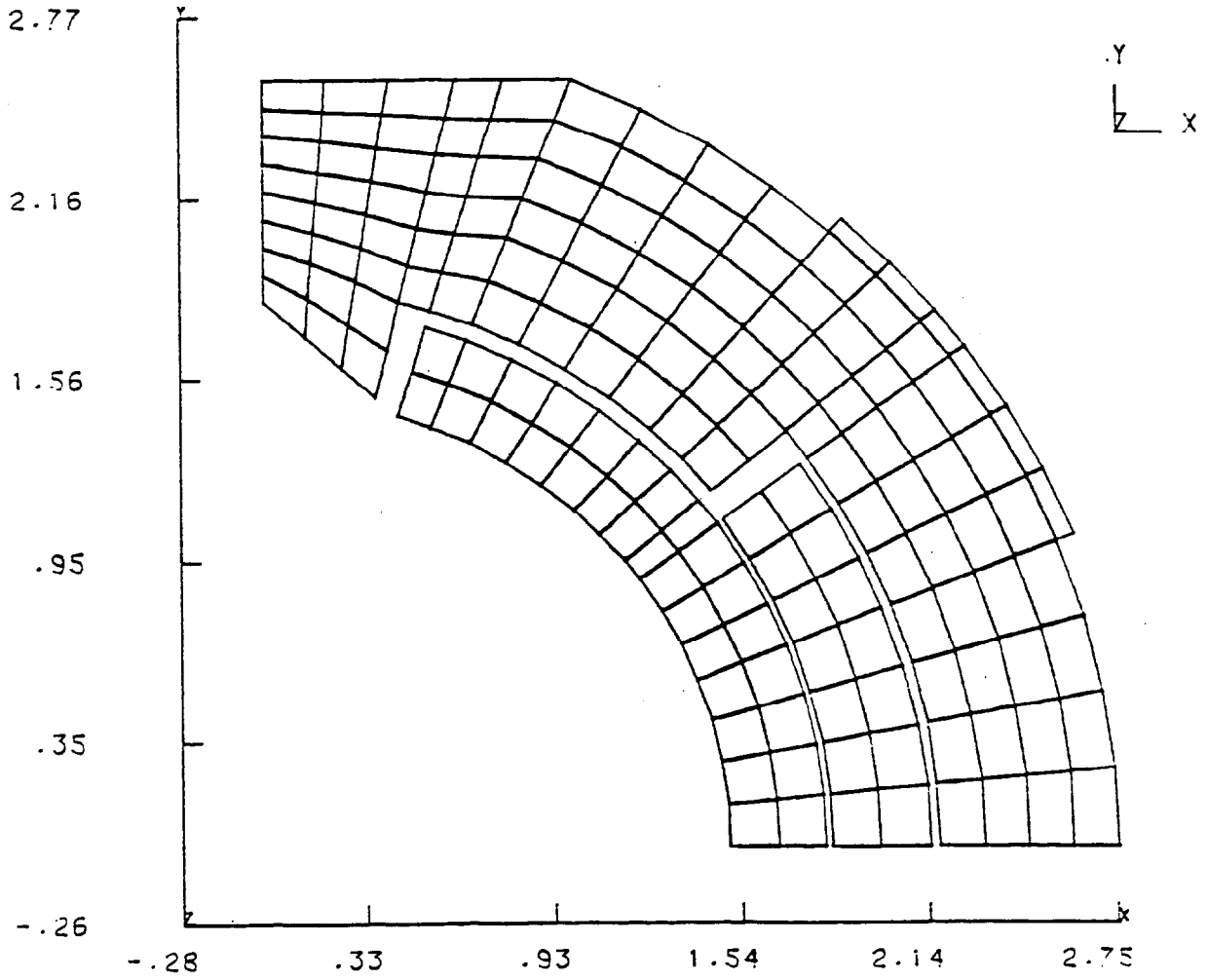

Displacement (mils)

Fig. 14 Horizontal displacement of collar on the median plane

E/S dipole

⊙ B=4.3 T

Present proposed high field dipole
Inner diameter 2.25"

B=10 T ⊙ B=4.0 T

⊙

fixed

open collar

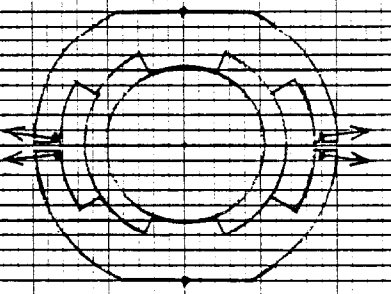

Case B

Present proposed high field dipole
Inner diameter 2.25"

E/S dipole

B=10 T △ △ B=4.3 T
△ B=4.0 T

KEK model dipole

B=6.7 T △

B=5.0 T △

Completely connected collar

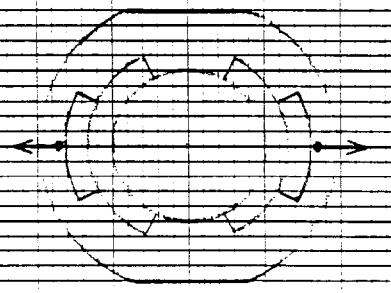

Case A

0 1 2 3 4 5 6

Inner diameter, inches

measurement was made on displacement of the collar at KEK and the horizontal displacement was 3.6 mils at room temperature for the externally applied force, which corresponded to magnetic force at 5T. Displacements of actual collars are, therefore, supposed to be 15 to 20% larger than predicted by the calculation in case A. The following calculation was made with the assumptions similar to those of case A.

Azimuthal displacement resulting from the magnetic force is shown in Figure 15, where triangular points stand for displacement without preload and circular points correspond to those with. The preload is equivalent and opposite to the magnetic force at the operational current. The elastic modulus of windings at cryogenic temperature was taken to be 2 to 3Mpsi for the E/S and KEK model dipole magnets. One can see from the results for the E/S dipole magnet that the azimuthal displacement of a preloaded magnet has a slight dependence on the elastic modulus of the winding, while that of unpreloaded magnets depends largely on the modulus. Basically the azimuthal displacement after preload is dependent mainly on the strength of the collar.

For the KEK model dipole magnet, there is a large difference between displacements in unpreloaded and preloaded cases. This is a result of the much larger circumference of the windings of the KEK model dipole magnets.

Although the preload decreases the azimuthal displacement as shown in Figure 15, it does not change the horizontal displacement of collar on the median plane.

2.3 Displacement of high field magnet.

The horizontal and azimuthal displacements that are shown in Figures 14 and 15 are both tolerable, being about 3 mils for a shell-type magnet of 4 to 5T range. Experimental results at LBL[7] and KEK show

Displacement, mils

Fig. 15 Azimuthal displacement of the most inner shell with and without preload

△ without preload
⊙ with preload

KEK model dipole
I = 6.8 kA (1.8 K)
B = 6.7 T
E = 3 Mpsi

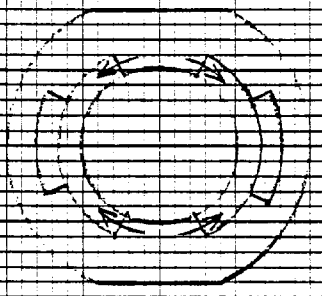

High field
I = 5 kA
B = 10 T
E = 6 Mpsi

E/S
I = 4.3 kA
B = 4.3 T

△ E = 2 Mpsi

△ E = 3 Mpsi

KEK model dipole
I = 4.9 kA
B = 5 T
E = 3 Mpsi

0 1 2 3 4 5 6 7 8 9

Inner diameter, inches

that excitation in pressurized helium II (1.8K) could increase the quench current by about 30% for magnets which achieve their short sample currents in helium I (4.2K) within a relatively small number of training quenches. Since the magnetic force in the winding increases as the square of transport current, the force at the quench current in helium II is 1.7 times larger than that in helium I, and accordingly the displacement should increase in the same proportion. The critical current of NbTi increases by 30 to 40% on such magnet load lines, with decreasing temperature of 4.2 to 1.8K. The increase of quench current is almost the same as that of critical current and, therefore, indicates a possible positive effect of superfluid on coil stability. However, to date no dipole magnets have been fabricated and operated at 10T. The value of 3 mils was taken as the tolerable displacement at 10T in pressurized helium II for field shape reasons.

Basic collar geometries for three different kinds of inner diameters were considered and are listed in Table IV. Parameters are explained in the inset. A displacement solution for a magnet whose inner diameter is 2.25 inches is plotted in Figure 16, with the condition of no preload. The original shape is indicated by dashed lines and the displacement is exaggerated by a factor of 10 for clarity. Numbers in Figure 16 show the values of displacement in units of mils (10^{-3}inch). The horizontal displacement of the inner edge of the collar on the median plane is 3 mils and shown as case A in Figure 14. The maximum azimuthal displacement is 4.5 mils and occurs in the inner shell. That value is indicated by a triangular mark in Figure 15.

Displacements caused by various preloads are shown in Figure 17 in terms of "relative"load, i.e., the applied preload divided by the total magnetic compressive force on the median plane at 5kA/turn. This Figure indicates that the preload increases the azimuthal

TABLE IV

BASIC DIMENSIONS OF COLLAR

	Magnet inner diameter (in.)		
	2.0	2.25	2.5
r_i (in.)	1.0	1.125	1.25
r_2	1.48	1.62	1.74
r_3	1.81	1.94	2.06
r_4	2.14	2.27	2.39
r_5	2.47	2.60	2.72
$r_6=r_5+t$	3.60	3.90	4.25
t	1.13	1.30	1.53
θ_1 (deg.)	81.4	81.2	81.1
θ_2	57.0	58.3	59.8
θ_3	42.6	41.6	41.0
θ_4	39.4	38.6	38.2
θ_5	70.0	70.0	70.0

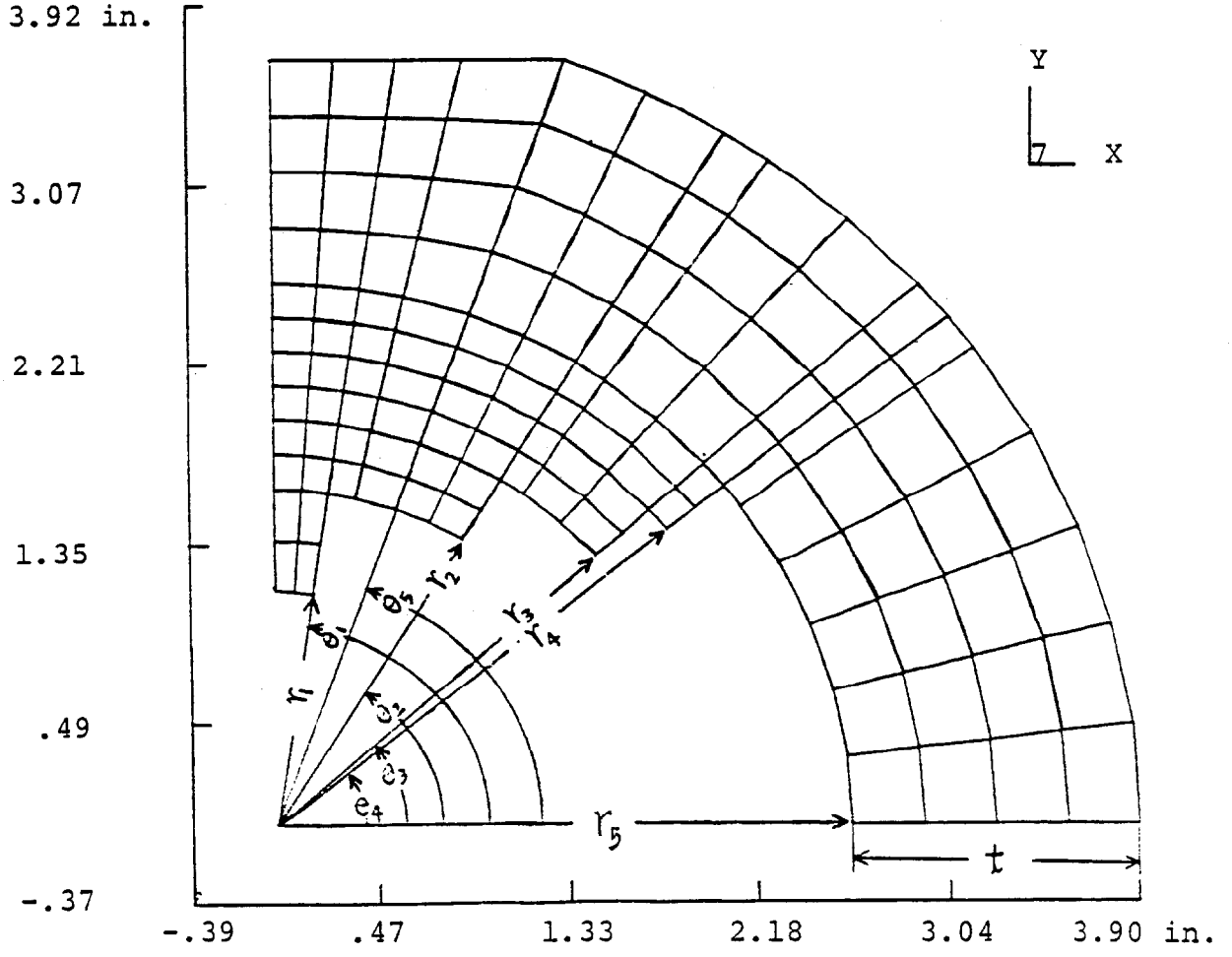

2.25 IN. DIPOLE MAG RUN 3. TH=1.30 IN. COIL E=6.E6GEOMETRY ANSYS

Fig. 16 Displacement of a high field magnet

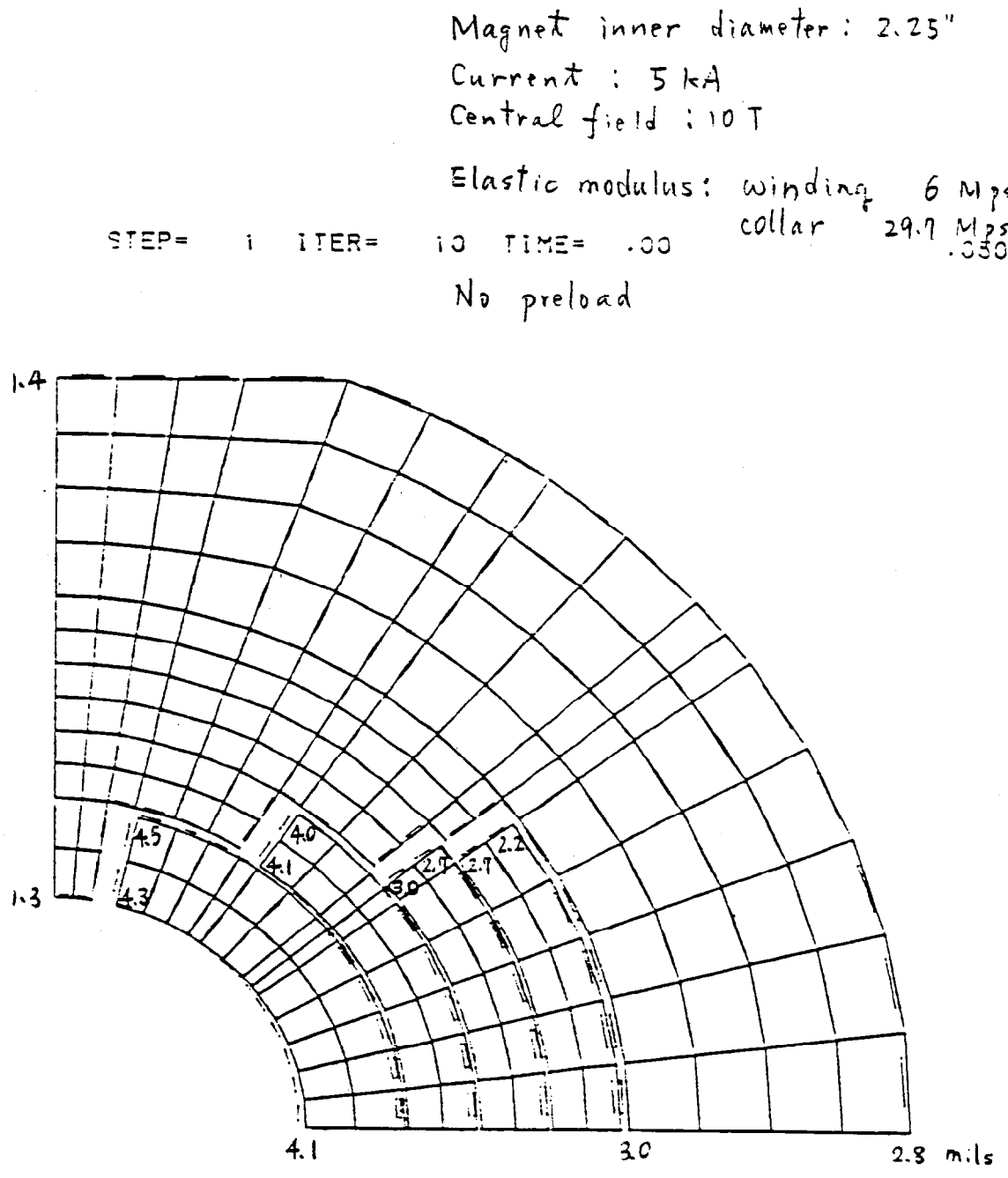

Fig. 17 Preload effect on displacement

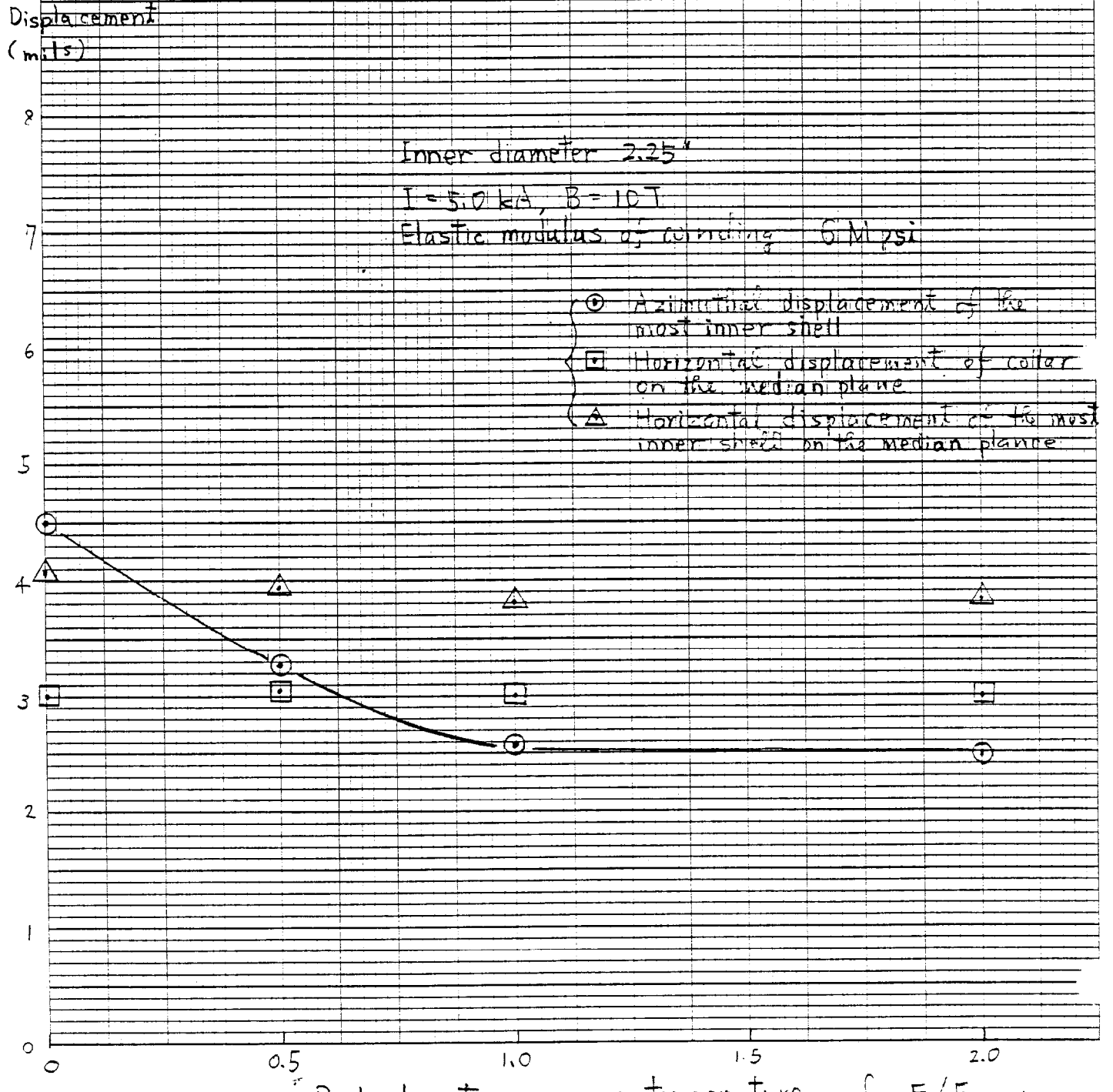

displacement until this displacement is constant for a relative preload greater than unity.

The dependence of displacement on "collar shape" is shown in Figure 18 for a magnet whose inner diameter is 2.25 inches. In the left half of the Figure, azimuthal and horizontal displacements are plotted as a function of collar thickness. An increase of collar thickness by 18% decreases the azimuthal displacement caused by the preload by 18% and the horizontal by 17%.

An effect of the thickness of the top region is shown in the left half. The thickness of the top region of the collar controls the azimuthal displacement of the inner shell under a given preload condition. This is because a given preload will result in a larger vertical displacement for a thinner top section collar.

2.4 Stress consideration.

The stress obtained in the collar and winding is shown in Figures 19 and 10, respectively. Equivalent stress, σ_e, is defined as $\sigma_e = (\sigma_1^2 - \sigma_1\sigma_2+\sigma_2^2)^{1/2}$ where σ_1 and σ_2 are the principal stress. This equivalent stress is plotted for high field dipole magnets of three different inner diameters and for the E/S dipole magnet for comparison, and is shown for the collars in Figure 19. Locations where the stress is obtained are indicated by letters which are explained on the inset. If there is a high stress near a specified location, that stress is shown by the symbol with a dash. Because of the simple geometry assumed for collars, the stress at locations I and O in Figure 19 is not accurate. The actual collar's stress depends on the welding, punched hole and/or key bar which is used in its assembly.

The calculated results are divided into three cases. The first is a calculation of stress during excitation of magnets with no preload. The locations indicated by C2 and C4 have a peak stress of about 20kpsi.

The second case is that of stress in preloaded

Fig. 18 Dependence of displacement on collar shape

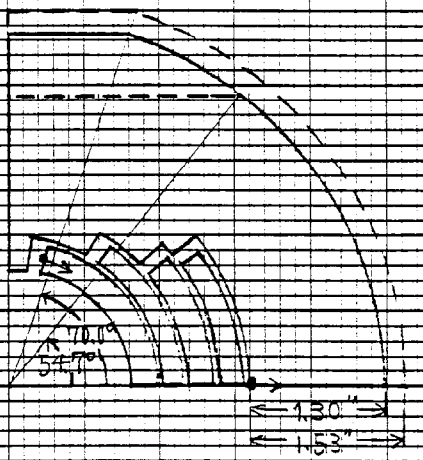

Displacement (mils)

I. Dependence on thickness of collar

II. Dependence on key angle of the flat top surface

Azimuth. displ. of the most inner shell, no preload

Horiz. displ. of collar on the medium plane, preload and no preload

Azimuth. displ. of the most inner shell, preload

0 1 2 3 4 5 6 7 8

1.0 1.2 1.4 1.6 1.8

40 50 60 70 80

Thickness on the median plane (inches)

Angle (degrees)

Fig. 19 Stress in collars

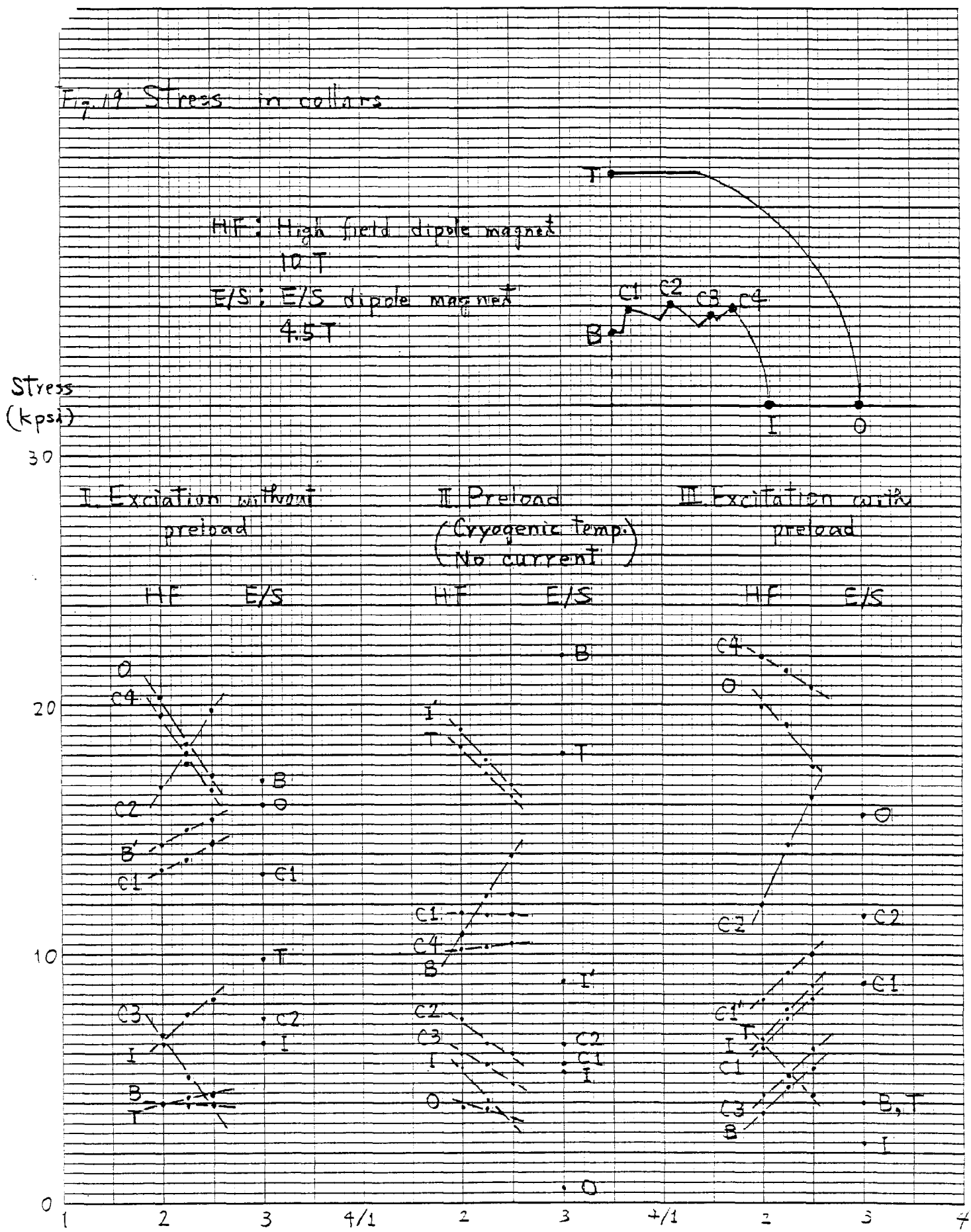

magnets at cryogenic temperatures. The preload was applied that would result in a prestress equal and opposite to the operational field's magnetic force. The stress shown in the Figure is a little lower in high field dipole magnets than in the E/S dipole magnet. A contour map of the equivalent stress is shown in Figure 20 for a 2.25 inch i.d. high field magnet. The contour lines are in units of 1.6kpsi. The Figure indicates that the stresses at the corner of C1 to C4 are relatively low compared with those in the top region. The horizontal component σ_x of stress along the vertical plane is given in the inset. The compressive stress is dominant in the lower region of the vertical plane and the tensile stress in the upper region. The total force on this plane is cancelled out by the sum. The vertical component σ_y of stress along the median plane is also plotted in the same Figure.

The third case in Figure 19 shows the stress which is caused by superposition of the preload and magnetic force. The stress in location C4 is on the order of 21 to 22kpsi. The corresponding contour lines are shown in Figure 21 for the 2.25 inch i.d. high field magnet. The stress is highly concentrated around the corner (C4) near the outer shell. Tensile stress is dominant in almost the entire region on the vertical and median planes. The total vertical repulsive force on the median plane is nearly equal to that in Figure 20.

The stress dependence as a function of collar shape is shown in Figure 22 and this Figure corresponds to stress levels of Figure 20. In the left half of Figure 22, the effective stress is plotted as a function of collar thickness on the median plane. Dashed and solid lines stand for central fields of zero and 10T, respectively (i.e., dashed lines correspond to the second case in Figure 19). The thicker collar decreases the stress concentration at the C4 location.

Fig. 20 Contour lines of equivalent stress in a preloaded high field magnet

Magnet inner diameter 2.25"
Preload: corresponding to force at 10T
Unit of contour lines : 1.6 kpsi

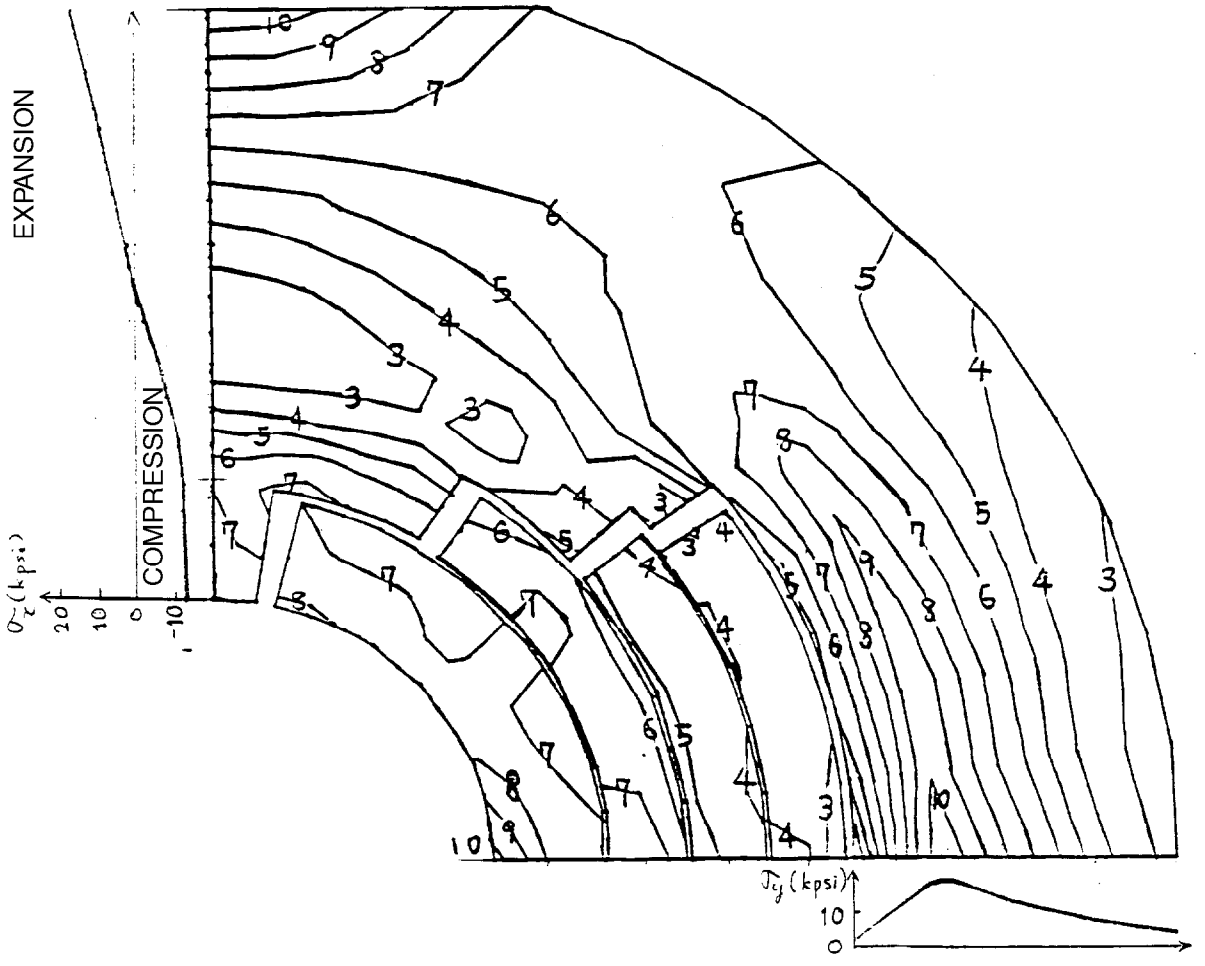

Fig. 21 Contour lines of equivalent stress in a preloaded high field magnet at a field of 10 T

Magnet inner diameter 2.25"
Preload: corresponding to force at 10 T
Current: 5.0 kA
Unit of contour lines: 1.5 kpsi

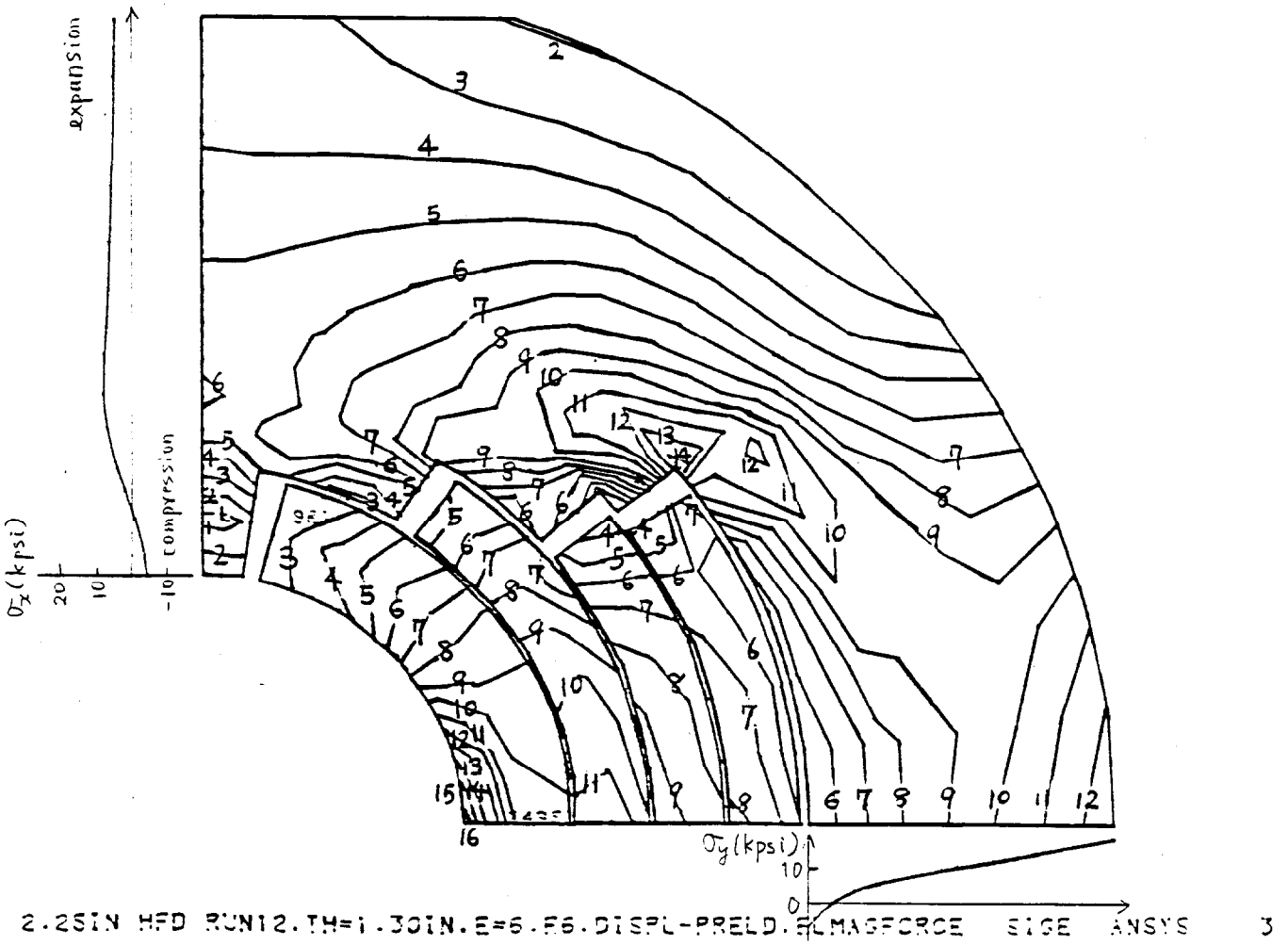

Fig. 22 Dependence of equivalent stress on collar shape

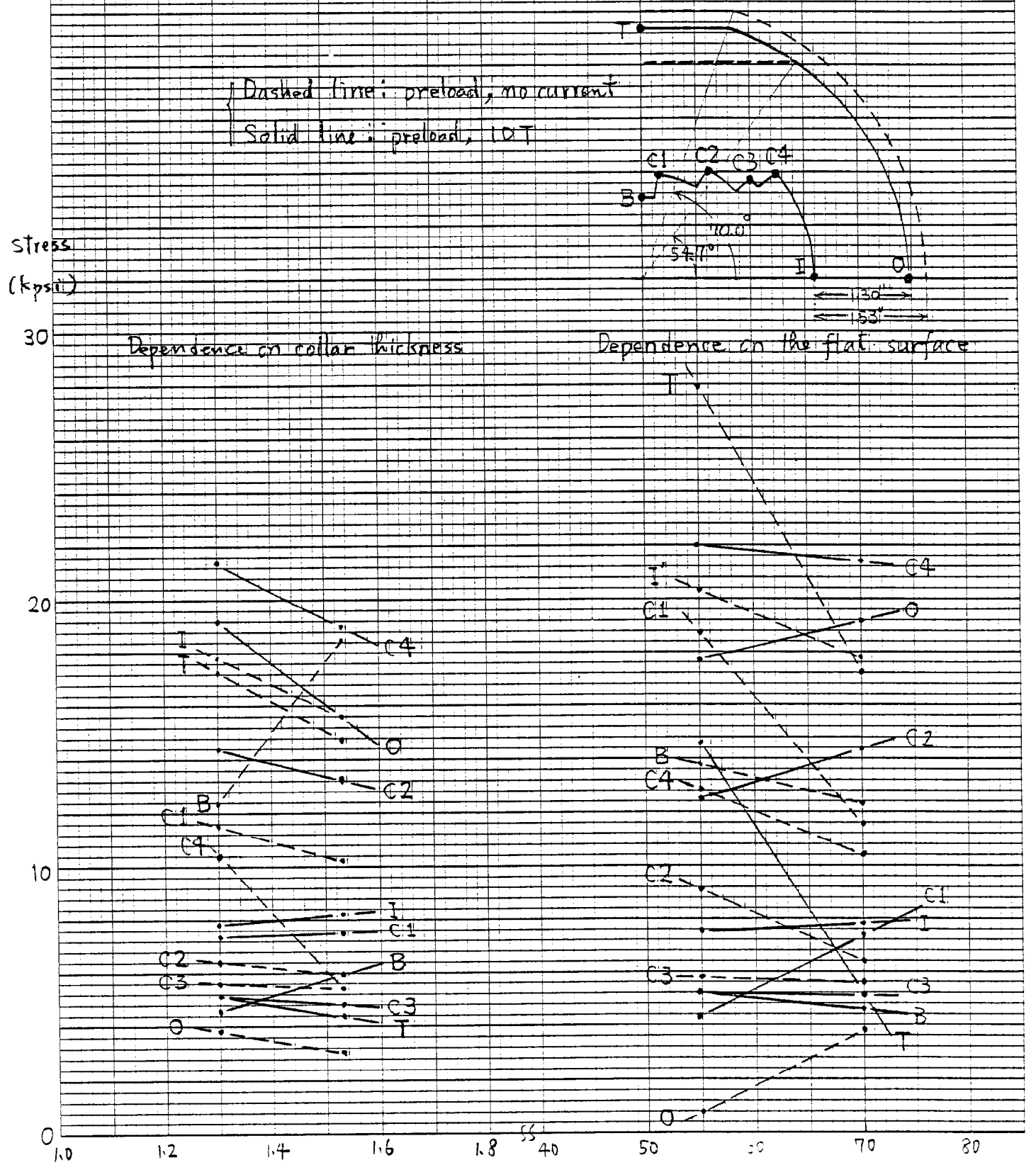

The right half shows dependence of the flat surface region. The thinner the collar thickness on the vertical plane the greater the stress concentration, particularly in the "T" location when the magnet is under preload.

Collar failures may have two sources. The first is a failure (fracture) at a time of preload at room temperature. Figure 23 shows the addition necessary to the circumferential length of the shells to results in a compressive force equal to the 10T magnetic force. The circular and triangular marks stand for the deflected circumferences obtained with elastic moduli of 6 and 3Mpsi, respectively. Since the elastic modulus of stainless steel is almost constant in the range from room to liquid helium temperature, those marks are equally valid for either room or liquid helium temperature. Because there is no glass-epoxy in the winding, the difference in the circumference caused by cooling between collar and shell on an ideal stress-free condition would be about 2 mils (loose). Therefore, the needed preload at room temperature to result in an equivalent preload corresponding to the magnetic force at 1.8K and 10T is similar to that in the second case presented in Figure 19, neglecting any possible creep effect in the winding. As listed in Table V, 304N stainless steel has a 0.2% yield strength of 50kpsi at room temperature. It therefore appears that the steel will tolerate the preload at room temperature for a properly designed collar.

Another collar failure possibility is a fracture of the collar due to fatigue caused by the cyclic field excitation. The highest stress in Figure 19 is 21 to 22kpsi. This stress is less than one-fifth of the 0.2% yield strength of 304N stainless steel at cryogenic temperature, which is normally used as a general rule of thumb in such cases. Therefore, the material should be tolerant of that stress level. However, there exist differences between the stress distributions of the simplified calculation and those of the actual collars, therefore further detailed calculations and experimen-

Fig. 23 Additional circumference needed to produce pressure corresponding electromagnetic force at 10 T

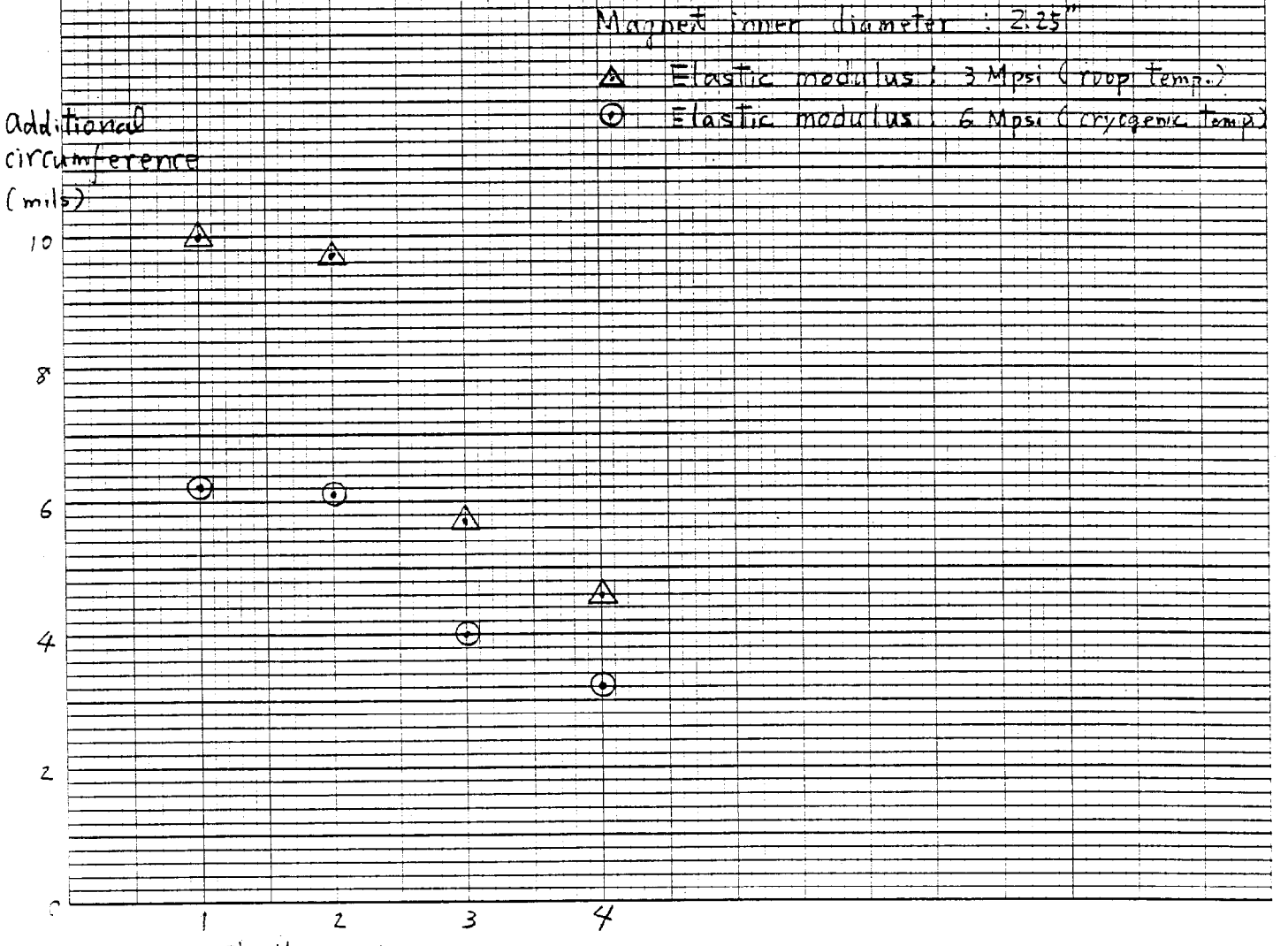

TABLE V

MECHANICAL PROPERTIES OF STAINLESS STEEL

	304N SS			$32\%M_n$-7%Cr Austenitic steel[5]
	4.2K	77K	293K	4.2K
0.2% yield strength (kpsi)	(160)	120	50	160
Tensile strength (kpsi)	(260)	220	100	210
Young's Modulus (Mpsi)	(30)		29	31

tal studies are required to determine the actual safety margins.

CONCLUSION

The following results were obtained in this study on the 4-shell-type 10T dipole magnet:

1. On the basis of presently attainable critical current densities of superconductor, the conductor is 33 strand NbTiTa cable for the inner shell, and 23 strand NbTi cable for the other shells would suffice.

2. The magnet inner diameter can be as small as 2 inches.

3. Although the magnetic force is large compared with other existing magnets, it seems possible to contain it by relatively thin collars. Further stress analysis is needed for details of the actual collar design used.

REFERENCES

1. D.C.Larbalestier, "Superconducting Materials - A Review of Recent Advances and Current Problems in Practical Materials", presented at the 8th International Conference on Magnet Technology, Karlsruhe, W.Germany, March 1981.

2. M.Wake, Private communication, August 1981.

3. C.Taylor et al., "A Novel Epoxy-free Construction Method For Fabricating Dipole Magnets and Test Results", presented at the 1981 Particle Accelerator Conference, Washington, D.C., March 1981; also LBL-11752.

4. C.E.Taylor and R.B.Meuser, "Prospects For 10T Accelerator Dipole Magnets", presented at the 1981 Particle Accelerator Conference, Washington, D.C., March 1981.

5. H.Hirabayashi et al., "A Design Proposal For High Field Dipole Magnet", KEK 81-1.

6. S.Mitsunobu et al., "A Test Dipole Magnet For the TRISTAN Superconducting Proton Ring", presented at the 1981 Particle Accelerator Conference, Washington, D.C., March 1981.

7. R.Althaus et al., "Performance of Dipole Magnet in Helium II", presented at the 1981 Particle Accelerator Conference, Washington, D.C., March 1981.

APPENDIX

HARMONIC COEFFICIENTS BY WINDING ERRORS

The magnetic field in a magnet bore tube can be expressed as

$$B_y + iB_x = \sum_{n=1}^{\infty} C_n z^{n-1} \tag{1}$$

where $z = x + iy$

The complex coefficient C_n is written for a shell shown in Figure A1-a as

$$C_n = -\frac{\mu_0}{2} J_n R_n \tag{2}$$

where $$J_n = \frac{1}{\pi} \int J e^{-in\theta} d\theta \tag{3}$$

$$= \frac{4J}{\pi} (\sin n\theta_2 - \sin n\theta_1) \tag{4}$$

$$R_n = \int_{r_1}^{r_2} \frac{1}{r^{n-1}} \left\{ 1 + \left(\frac{r}{r_i}\right)^{2n} \right\} dr \tag{5}$$

$$= \begin{cases} \frac{1}{n-2} \left\{ \frac{1}{r_1^{n-2}} - \frac{1}{r_2^{n-2}} \right\} + \frac{1}{r_i^{2n}} \frac{r_2^{n+2} - r_1^{n+2}}{n+2} & n \neq 2 \\ \log \frac{r_2}{r_1} + \frac{1}{r_i^4} \frac{r_2^4 - r_1^4}{4} & n = 2 \end{cases} \tag{6}$$

The harmonic coefficients are defined as

$$b_{n-1} + i a_{n-1} = C_n / C_1 = C_n / B_0 \tag{7}$$

where B_0 is the central field.

If there is a small displacement in winding, its effect is written as

$$\Delta C_n = -\frac{\mu_0}{2} \left\{ J_n \Delta R_n + R_n \Delta J_n \right\} \tag{8}$$

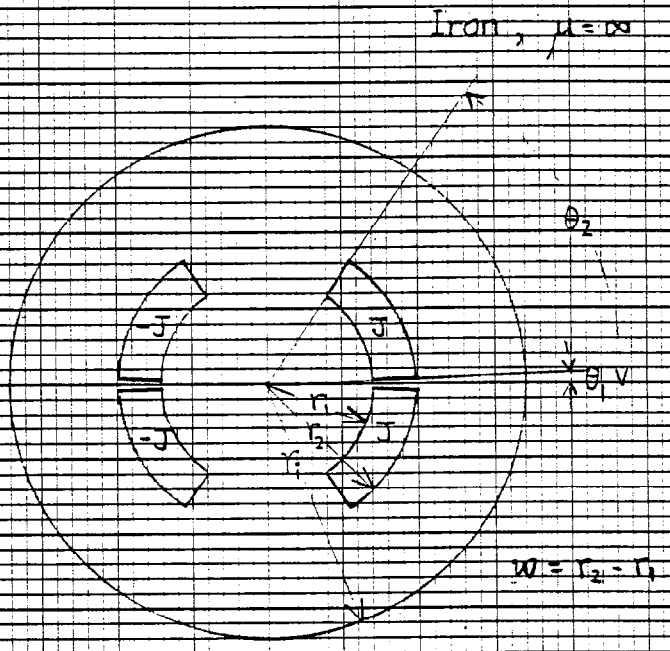

(a) Basic geometry

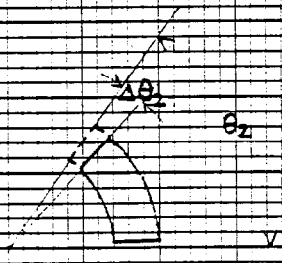

(b) Azimuthal displacement

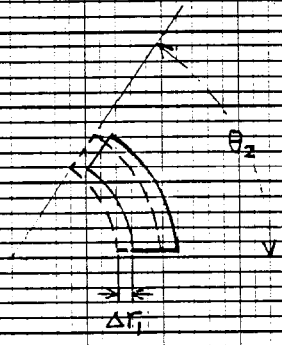

(c) Horizontal displacement

Fig. A-1 Harmonics calculation

For a small azimuthal change of the winding in the first quadrant shown in Figure A1-b, the factor of ΔJ_n is written as

$$\Delta J_n = \left.\frac{\partial J_n}{\partial \theta_2}\right|_{\text{first quadrant}} \cdot \Delta\theta_2$$

$$= \frac{J}{\pi}\left\{ e^{-in\theta_2} - \frac{i}{\theta_2 - \theta_1}\,\frac{e^{-in\theta_2} - e^{-in\theta_1}}{n} \right\}\cdot \Delta\theta_2 \qquad (9)$$

If the angle θ_2 changes in all the quadrants by the same amount $\Delta\theta_2$, Eq. (9) is expressed as

$$\Delta J_n = \frac{4J}{\pi}\left\{ \cos n\theta_2 - \frac{\sin n\theta_2 - \sin n\theta_1}{n(\theta_2 - \theta_1)} \right\}\cdot \Delta\theta_2 \,, \quad n = \text{odd} \qquad (10)$$

The first and second terms correspond to change of the angle and current density.

For a small horizontal change of the winding in the first quadrant shown in Figure A1-c, the effects are written as follows:

$$\Delta R_n = \left.\frac{\partial R_n}{\partial r_1}\right|_{\text{first quadrant}} \cdot \Delta r_1$$

$$= \left\{ r_2^{1-n} - r_1^{1-n} + \frac{1}{r_i^{2n}}\left(r_2^{n+1} - r_1^{n+1} \right) \right\}\cdot \Delta r_1 \qquad (11)$$

$$\Delta J_n = \left.\frac{\partial J_n}{\partial r_1}\right|_{\text{first quadrant}} \cdot \Delta r_1$$

$$\simeq \frac{J}{\pi} e^{-in\theta_2}\left\{ - \frac{\theta_2 - \theta_1}{r_1 + \frac{w}{2}} \right\}\cdot \Delta r_1 \qquad (12)$$

If the windings in all quadrants move by the same amount, Eqs. (11) and (12) can be written as

$$\Delta R_n = 4\left\{ r_2^{1-n} - r_1^{1-n} + \frac{r_2^{n+1} - r_1^{n+1}}{r_i^{2n}} \right\}\cdot \Delta r_1 \qquad (13)$$

$$\Delta J_n = \frac{4\cos n\theta_2}{\pi}\left\{ - \frac{\theta_2 - \theta_1}{r_1 + \frac{w}{2}} \right\}\cdot \Delta r_1 \qquad (14)$$